A 0.18-μg Bias-Instability 0.8-μg/$\sqrt{\mathrm{Hz}}$ Resolution Silicon Oscillating Accelerometers with Low-Hysteresis Temperature Extraction and On-Chip Learning-Based Compensation

Yuchi Zou[1,2], Benhao Huang[2], Yuwei Huang[2], Yang Bo[2], Jing Zhang[3], Longyang Lin[4], Jian Zhao[1]
[1]National Key Laboratory of Science and Technology on Micro/Nano Fabrication, Shanghai Jiao Tong University, China.
[2] School of Integrated Circuits, Shanghai Jiao Tong University, China.
[3]School of Mechanical Engineering, Nanjing University of Science and Technology, China.
[4]School of Microelectronics, Southen University of Science and Technology, China. (Email: zhaojianycc@sjtu.edu.cn)

***Abstract*—Temperature drift remains a major limitation to the long-term stability of silicon oscillating accelerometers. Conventional compensation techniques encounter two critical challenges: (1) hysteresis-induced errors in in-situ temperature measurements, and (2) time- and environment-dependent variations in compensation model coefficients, which hinder complete drift cancellation. This work introduces two key innovations to address these issues. First, a digitally programmable gain amplifier enables real-time measurement of the MEMS resonator's quality factor, allowing low-hysteresis temperature estimation by directly linking the resonator amplitude to its structural temperature. Second, a recursive least squares on-chip learning algorithm adaptively updates the compensation coefficients over time, effectively modeling temperature dependencies and suppressing long-term drift. The proposed readout integrated circuit, fabricated in a 0.18-μm CMOS process, integrates MEMS sensing and compensation functionalities. Experimental results demonstrate a bias instability of 0.18 μg and a noise density of 0.8 μg/$\sqrt{\mathrm{Hz}}$. These results validate the framework's capability for high-precision inertial sensing in UAVs, UUVs, and compact navigation systems operating under dynamic environmental conditions.**

Index Terms*—Silicon Oscillating Accelerometer, Readout Integrated Circuits, Low-hysteresis temperature extraction, Temperature Compensation

I. INTRODUCTION

The silicon oscillating accelerometer (SOA) is a class of high-precision microelectromechanical systems (MEMS) accelerometers characterized by unique time-modulated sensing mechanisms. These features, along with their miniaturization potential, position SOAs as a promising solution to bridge the gap between low-cost MEMS capacitive accelerometers and bulky quartz flexure accelerometers. As a result, SOAs are well suited to meet the urgent demand for navigation-grade inertial performance in compact platforms such as unmanned underwater vehicles (UUVs), unmanned aerial vehicles (UAVs), and smart munitions [1].

However, the bias stability of SOAs is still limited by the intrinsic properties of silicon and the related fabrication and packaging processes, resulting in a performance gap compared to quartz-based accelerometers [2]. A key challenge is temperature drift, caused by variations in silicon's Young's modulus and thermally induced stresses under changing ambient conditions [3]. A common strategy to mitigate this drift is to use an auxiliary temperature sensor. As shown in Fig. 1(a), this approach has two main issues. First, accurate in-situ temperature measurement is difficult because the sensor is spatially separated from the resonator, leading to hysteresis during thermal transients. Second, silicon resonators exhibit less stable temperature coefficients over time than quartz, due to environmental fluctuations and stress relaxation [2].

This work proposes a dedicated readout integrated circuit (ROIC) that enables temperature drift compensation through two key innovations. First, an automatic amplitude control (AAC) loop with built-in Q-factor measurement extracts temperature information with minimal hysteresis. Second, a recursive least squares on-chip learning (RLS-OCL) algorithm continuously updates the polynomial coefficients for temperature compensation, based on zero-bias outputs recorded during sensor idle periods. The proposed ROIC achieves a relative bias instability of 1.8 ppb and a noise density of 8 ppb/$\sqrt{\mathrm{Hz}}$. These results highlight the potential of SOAs for long-term, high-precision navigation applications.

The remainder of this paper is organized as follows. Section II presents the system architecture and circuit-level implementation of the proposed ROIC. Section III reports the experimental results and compares the performance with state-of-the-art works. Finally, Section IV concludes the paper.

II. PROPOSED MEMS READOUT INTERFACE CIRCUIT

Fig. 1(b) shows the block diagram of the proposed ROIC, which interfaces with the MEMS sensor to form the complete SOA system. Under acceleration, the resonant frequencies of the two differential resonators shift in opposite directions, and their difference, Δf, directly represents the input acceleration. Each resonator, along with the transimpedance amplifier (TIA) and digitally programmable gain amplifier (DPGA), forms a resonance-sustaining loop controlled by the AAC circuit

Yuchi Zou and Benhao Huang contribute equally to this work.

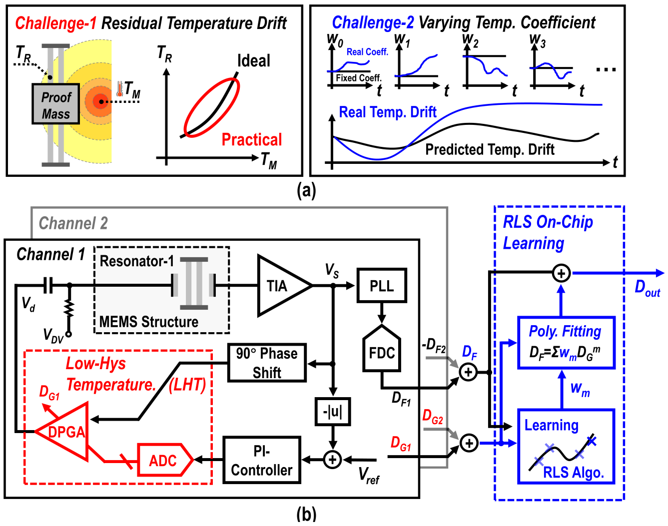

Fig. 1. (a) Challenges in temperature compensation. (b) System-level block diagram of the proposed ROIC.

to maintain constant signal amplitude. The TIA output V_s is frequency-multiplied by a phase-locked loop (PLL) and digitized by the FDC into D_{F1} and D_{F2}, which carry frequency information. The ADC outputs D_{G1} and D_{G2} reflect the resonator's Q-factor, enabling low-hysteresis temperature sensing. Using the time period when the accelerometer is stationary, the RLS algorithm is initiated to fit the relationship between D_G and D_F (the relationship between temperature and frequency drift) and update the polynomial coefficients w_m. When the accelerometer begins to operate (with a non-zero input), the update of w_m is stopped, and w_m is used to compensate for frequency drift using D_G.

Fig. 2(a) shows the proposed MEMS resonator driving circuit, which includes the resonance-sustaining loop and the AAC circuit. The resonance-sustaining loop, consisting of the MEMS resonator, TIA, and DPGA, maintains oscillation via a unity-gain feedback loop. The AAC circuit comprises a buffer, rectifier, subtractor, high-linearity voltage-to-current converter (G_m), loop filter, 6-bit SAR ADC, and DPGA. It regulates the signal amplitude V_S to a reference value V_{REF} and uses chopping to suppress low-frequency noise. Fig. 2(b) presents the small-signal model of the AAC loop in the steady state [4], from which the relationship between the ADC output D_G and the Q-factor is derived. As the Q-factor is proportional to the in-situ temperature T_R of the MEMS structure, embedding the ADC in the AAC loop enables direct temperature inference from D_G, achieving low-hysteresis temperature sensing with inherent noise shaping.

The functional diagram of the proposed RLS-OCL temperature compensation module is shown in Fig. 3. This module has 4 inputs which are the frequency and digital gain control code of the DPGA from the two channels. Subsequently, the downsampled frequency difference D_{F_CIC} and average gain control code D_{G_CIC} are recorded in registers and subtracted their initial values to remove large static components and reveal smaller dynamic components. Then, both D_{G_CIC} and D_{F_CIC} are converted to 32-bit floating-point before fed

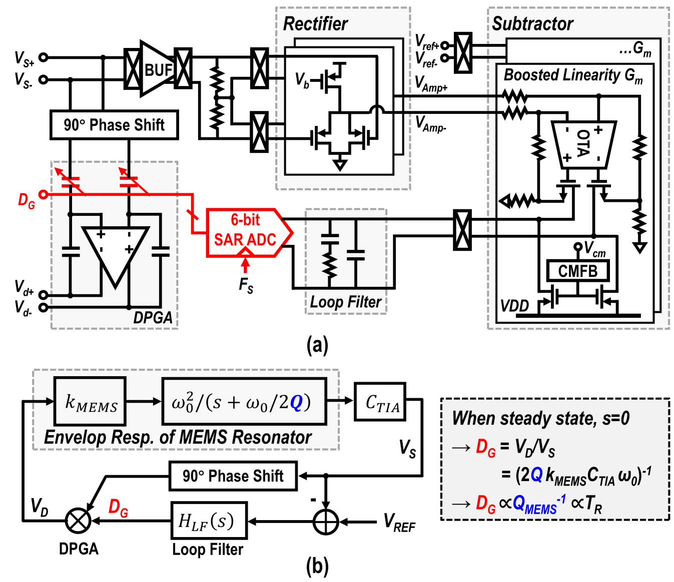

Fig. 2. (a) Proposed automatic amplitude control circuit with built-in low-hysteresis temperature indicator. (b) Relationship among D_G, Q, and T_R in the steady state.

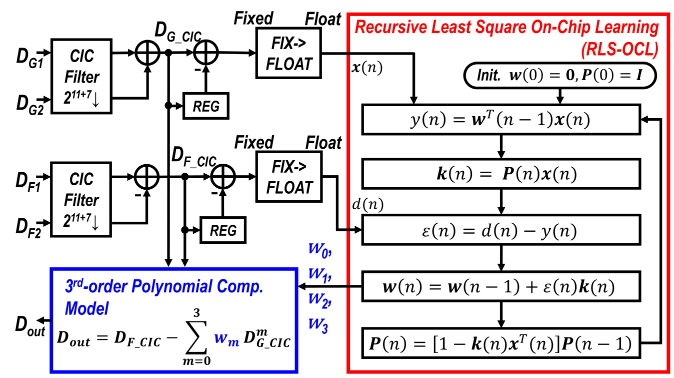

Fig. 3. Proposed recursive least-squares on-chip learning technique for dynamic temperature compensation model updating.

into RLS-OCL core, and serve as the independent variable x and the desired dependent variable d for the RLS algorithm, respectively. Initial values for the polynomial coefficient vector w and the covariance matrix P are set before the beginning of fitting. The RLS algorithm detects the error ε between the output dependent variable y, which is calculated based on the current w and x, and the desired dependent variable d. According to the least-squares criterion, it recursively updates the current optimal w and P and outputs w. Based on D_{G_CIC}, w, and the recorded initial values, the trend of D_{F_CIC} can be restored and predicted, enabling the adaptive temperature compensation. Compared to Least Mean Square algorithm, RLS algorithm allows data points to enter sequentially without the need to obtain all data points at once, which matches well with SOA's scenarios.

III. Measurement Results and Performance Comparison

The proposed readout circuit was fabricated using a 0.18-μm CMOS process and occupies an active area of 13.5 mm^2.

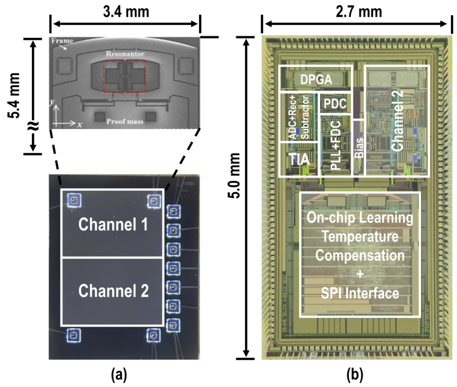

Fig. 4. Die photographs of (a) MEMS accelerometer [5] and (b) CMOS ROIC.

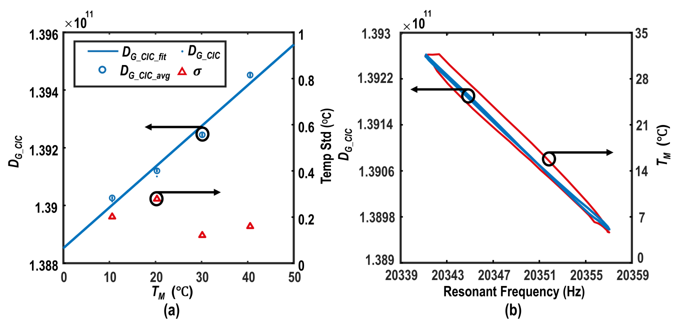

Fig. 5. Temperature sweeping tests: (a) static temperature sweeping, and (b) dynamic temperature cycling.

The die photograph is shown in Fig. 4. The measurement procedures are described as follows.

To evaluate the effectiveness of D_{G_CIC} in representing low-hysteresis temperature behavior, a steady-state temperature sweep test was performed. The temperature chamber was programmed to increase from 10°C to 40°C in increments of 10°C. At each step, after a 20-minute stabilization period, the reference thermometer (T_M), positioned close to the MEMS sensor chip, and D_{G_CIC} were recorded over a one-minute interval. Fig. 5(a) illustrates the correlation between the recorded values of T_M and D_{G_CIC}. Using T_M as the reference, the temperature resolution achieved by D_G was determined to be better than 0.3°C.

To further validate the low-hysteresis performance of D_{G_CIC}-based temperature monitoring, a rapid cyclic temperature sweep test was conducted. The temperature was cycled between 0°C and 35°C at a rate of 2°C/min, with one rising and one falling phase. During the entire process, both the reference thermometer (T_M) and D_{G_CIC} were continuously recorded. Fig. 5(b) compares the oscillation frequency as a function of D_{G_CIC} and T_M, respectively. The results confirm that D_{G_CIC} closely tracks the near in-situ temperature of the silicon resonator with minimal hysteresis. In contrast, T_M exhibits a significantly larger maximum hysteresis error compared to D_{G_CIC}.

Fig. 6 presents the evaluation of the proposed RLS-OCL temperature compensation method. In an 18-hour continuous test, the SOA was placed on a stationary surface and alternately operated in coefficient update mode (using the RLS algorithm) and normal operation mode. During the first 7 hours, natural room temperature fluctuations drove the convergence of the compensation coefficients w_m. When switched to operation mode, the coefficients were held constant to enable stable temperature drift compensation. This cycle was repeated four times, with the bias stability calculated for each operational phase. On average, the proposed method achieved a stability of 5.3 μg, representing 27× and 54× improvements over fixed-coefficient compensation and no compensation, respectively.

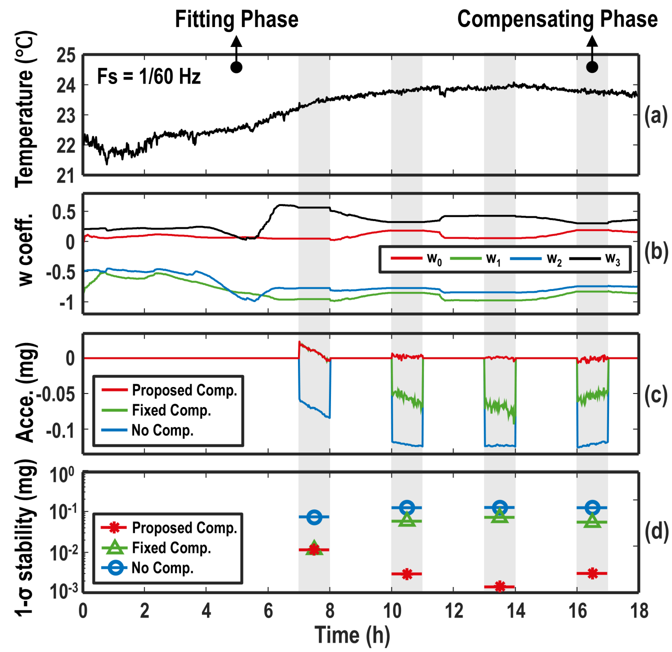

Fig. 6. The compensation performance of the temperature compensation digital circuit, with temperature ranging from 0°C to 30°C.

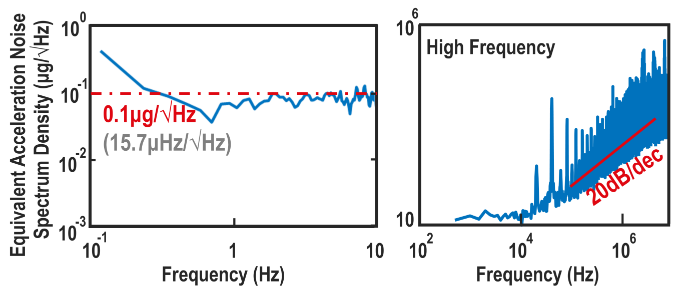

Fig. 7. The output power spectrum of the FDC.

The on-chip FDC was tested using a 20 kHz sinusoidal input generated by a signal generator. The equivalent acceleration noise spectrum is shown in Fig. 7, exhibiting a noise density of 0.1 μg/$\sqrt{\text{Hz}}$ at 10 Hz, which is lower than the overall acceleration noise level.

The full-scale range and nonlinearity of the SOA were measured using a high-precision centrifuge. As shown in Fig. 8, the nonlinearity was 140 ppm within the ±50 g range. Subsequently, static stability was evaluated by recording the zero-input output over a one-hour period. Both the Allan variance and power spectral density (PSD) were computed, as shown in Fig. 9(a) and (b), respectively. The measured bias instability is 0.18 μg at an averaging time of approximately 100 s, and the noise level is 0.8 μg/$\sqrt{\text{Hz}}$ at 0.2 Hz.

TABLE I
PERFORMANCE SUMMARY COMPARED WITH THE STATE-OF-THE-ART WORKS.

Parameter	ISS'15 [6]	JSSC'15 [8]	JSSC'20 [7]	JSSC'24 [9]	JSSC'17 [11]	ISS'17 [10]	Inertial'21 [12]	This work
Mechanism	Capacitive	Capacitive	Capacitive	Capacitive	SOA	SOA	SOA	SOA
Process(μm)	N.A.	0.5	0.13+0.35	0.18	0.35	N.A.	N.A.	0.18
Supply (V)	N.A.	7	1.4~12	1.8	1.5	3.3~5	N.A.	1.8
Full scale (g)	±15	±1.2	±0.55	±8	±30	±100	±60	**±50**
Power (mW)	400	23	17	0.23	2.7	100	<500*	14.5
Bias instability (μg)	0.8	18	/	4.1	0.23	0.3	0.4	**0.18**
Noise density (μg/√Hz)	1	0.2	0.022	25	1	8	10	**0.8**
Relative instability (ppb)	27	7500	/	256	4	1.5	3.3	**1.8**
Relative noise density (ppb/√Hz)	33	83	200	1560	17	40	83	**8**
On-chip Compensation	N.A.	N.A.	N.A.	N.A.	N.A.	Temp.	Temp.	**Temp.**

* This power is reported in a 6-axis IMU, the single sensor's power is less than 3Watts/6

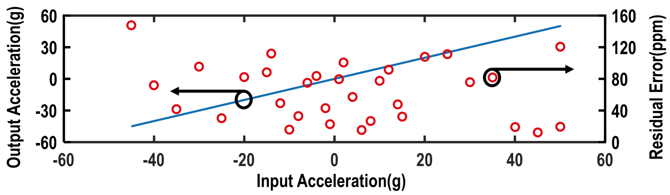

Fig. 8. Centrifugal testing results of the fabricated SOA.

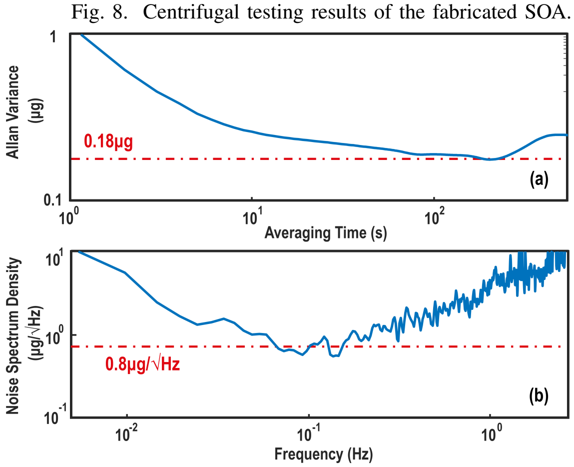

Fig. 9. (a) The test results of the Allan variance. (b) The output power spectrum of the SOA system.

Finally, Table I compares this work with prior art [2], [6]–[12]. Taking the full-scale range into account, the proposed SOA achieves a relative bias instability of 1.8 ppb and a relative noise density of 8 ppb/$\sqrt{\text{Hz}}$. Compared to other designs, this work demonstrates the lowest bias instability while maintaining moderate power consumption. In addition, it supports low-hysteresis temperature sensing and RLS-OCL-based temperature compensation, making it well suited for future long-duration applications.

IV. CONCLUSION

This work presents an integrated readout circuit for silicon oscillating accelerometers, featuring Q-factor-based low-hysteresis temperature sensing and on-chip learning-based compensation to mitigate temperature-induced bias drift. Measurements show the fabricated ROIC achieves bias instability as low as 0.18 μg and a noise floor of 0.8 $\mu\text{g}/\sqrt{\text{Hz}}$ over a $\pm$50 g full-scale range, while consuming only 14.5 mW. These results demonstrate the circuit's strong potential for navigation-grade applications in autonomous systems and other long-term precision sensing tasks.

REFERENCES

[1] S. Zotov, "A detailed journey from tactical to high-end navigation-grade mems accelerometers at emcore," in *DGON Inertial Sensors and Applications (ISA)*, 2024, pp. 1–19.

[2] S. Zotov, R. Moore, S. Shtigluz, J. Paxton, A. Popp, G. Smyers, H. Kwon, M. Frazee, T. Aston, D. Hoyh, and A. Lu, "Compact quartz mems imu: from tactical to navigation grade," in *DGON Inertial Sensors and Systems (ISS)*, 2021, pp. 1–19.

[3] N. Yazdi, F. Ayazi, and K. Najafi, "Micromachined inertial sensors," *Proceedings of the IEEE*, vol. 86, no. 8, pp. 1640–1659, 1998.

[4] J. Zhao, Y. Zhao, X. Wang, G. Xia, A. Qiu, Y. Su, and Y. P. Xu, "A system decomposition model for phase noise in silicon oscillating accelerometers," *IEEE Sensors Journal*, vol. 16, no. 13, pp. 5259–5269, 2016.

[5] J. Zhang, T. Wu, Y. Liu, C. Lin, and Y. Su, "Thermal stress resistance for the structure of mems-based silicon differential resonant accelerometer," *IEEE Sensors Journal*, vol. 23, no. 9, pp. 9146–9157, 2023.

[6] P. Ullah, V. Ragot, P. Zwahlen, and F. Rudolf, "A new high performance sigma-delta mems accelerometer for inertial navigation," in *DGON Inertial Sensors and Systems Symposium (ISS)*, 2015, pp. 1–13.

[7] Y. Furubayashi, T. Oshima, T. Yamawaki, K. Watanabe, K. Mori, N. Mori, A. Matsumoto, Y. Kamada, A. Isobe, and T. Sekiguchi, "A 22-ng/$\sqrt{}$ hz 17-mw capacitive mems accelerometer with electrically separated mass structure and digital noise- reduction techniques," *IEEE Journal of Solid-State Circuits*, vol. 55, no. 9, pp. 2539–2552, 2020.

[8] H. Xu, X. Liu, and L. Yin, "A closed-loop $\sigma\delta$ interface for a high-q micromechanical capacitive accelerometer with 200 ng/$\sqrt{}$hz input noise density," *IEEE Journal of Solid-State Circuits*, vol. 50, no. 9, pp. 2101–2112, 2015.

[9] J. Lin, L. Pham, R. Tao, A. Gutmann, S. Guo, A. Cywar, A. Spirer, J. Mansson, and K. Nguyen, "A low-power, wide-bandwidth, three-axis mems accelerometer asic using beyond-resonant-frequency sensing," *IEEE Journal of Solid-State Circuits*, vol. 59, no. 3, pp. 774–783, 2024.

[10] O. Lefort, I. Thomas, and S. Jaud, "To the production of a robust and highly accurate mems vibrating accelerometer," in *DGON Inertial Sensors and Systems (ISS)*, 2017, pp. 1–19.

[11] J. Zhao, X. Wang, Y. Zhao, G. M. Xia, A. P. Qiu, Y. Su, and Y. P. Xu, "A 0.23-μg bias instability and 1-μg/$\sqrt{}$hz acceleration noise density silicon oscillating accelerometer with embedded frequency-to-digital converter in pll," *IEEE Journal of Solid-State Circuits*, vol. 52, no. 4, pp. 1053–1065, 2017.

[12] B. Johnson, C. Albrecht, T. Braman, K. Christ, P. Duffy, D. Endean, M. Gnerlich, and J. Reinke, "Development of a navigation-grade mems imu," in *IEEE International Symposium on Inertial Sensors and Systems (INERTIAL)*, 2021, pp. 1–4.